Mol Neurobiol (2017) 54:6490–6506
DOI 10.1007/s12035-016-0136-4

# Anthocyanin-Loaded PEG-Gold Nanoparticles Enhanced the Neuroprotection of Anthocyanins in an $A\beta_{1–42}$ Mouse Model of Alzheimer's Disease

**Tahir Ali[1] · Min Ju Kim[1] · Shafiq Ur Rehman[1] · Ashfaq Ahmad[1] · Myeong Ok Kim[1]**

Received: 29 April 2016 / Accepted: 14 September 2016 / Published online: 11 October 2016


**Abstract** Nanomedicine is an emerging research area. In this study, we investigated the neuroprotective efficacy of anthocyanin-loaded polyethylene glycol-gold nanoparticles (PEG-AuNPs) for enhancing the neuroprotective efficacy of anthocyanins in an amyloid beta $(A\beta)_{1–42}$ mouse model of Alzheimer's disease. We observed that both anthocyanin-loaded PEG-AuNPs and anthocyanins treatment (12 μg/g/day for 14 days) ameliorated memory impairments in the $A\beta_{1–42}$-injected mice. However, the anthocyanin-loaded PEG-AuNPs were more effective than free anthocyanins. Anthocyanin-loaded PEG-AuNPs protected pre- and post-synaptic proteins from $A\beta_{1–42}$-induced synaptic dysfunction. Interestingly, the anthocyanin-loaded PEG-AuNPs also regulated the p-PI3K/p-Akt/p-GSK3β pathway and, as a result, prevented the hyperphosphorylation of tau protein at serines 413 and 404 in the $A\beta_{1–42}$-injected mice. Western blot results of cytochrome c, Bax/Bcl2, caspases and poly (ADP-ribose) polymerase-1 expression levels, and immunohistochemical Nissl and Fluoro-Jade B staining also indicated that the anthocyanin-loaded PEG-AuNPs inhibited apoptosis and neurodegeneration in the $A\beta_{1–42}$-injected mice. Our results suggest that the conjugation of dietary polyphenolic compounds with gold nanoparticles, such as anthocyanin-loaded PEG-AuNPs, is a novel approach that may represent an important and promising nanomedicine strategy to prevent age-associated neurodegenerative diseases.

Tahir Ali, Min Ju Kim, and Shafiq Ur Rehman equally contributed to this work.

✉ Myeong Ok Kim
mokim@gnu.ac.kr

[1] Division of Applied Life Science (BK21), College of Natural Sciences, Gyeongsang National University, Jinju 660-701, Republic of Korea

**Keywords** Alzheimer's disease · Nanomedicine · Anthocyanin-PEG-gold nanoparticles · Synaptic dysfunction · Neurodegeneration

## Introduction

Alzheimer's disease (AD), the most common neurodegenerative disease, is characterized by progressive memory impairment and cognitive abnormalities due to amyloid beta (Aβ) plaque deposition and neurofibrillary tangle formation in the brain [1, 2]. Brain Aβ peptide accumulation in the form of plaques and oligomers have been shown to play a critical role in AD pathogenesis, which includes neurodegeneration, synaptic dysfunction, neuroinflammation, and generation of reactive oxygen species [3–6]. Various drug delivery strategies have been adopted for controlled and targeted drug delivery to the brain to improve the treatment of various age-related neurodegenerative diseases such as AD [7, 8]. The use of gold nanoparticles (AuNPs) as a drug delivery system is a rapidly progressing field in the area of nanotechnology [9]. AuNPs have garnered significant attention and have been proven as an important tool for efficient drug delivery due to their unique properties such as their non-toxic nature and biocompatibility [10–12]. Various studies have reported the size-dependent in vivo distribution of AuNPs in organs and their transport through the blood-brain barrier (BBB), allowing them to reach and distribute throughout the brain; particularly, high concentrations have been detected in the hippocampal and cortical regions [13–19]. Among nanocarrier systems, polymeric nanoparticles (NPs) are promising agents that can open the BBB, prolong drug release, and avoid enzymatic degradation [20]. The active agents can be chemically coupled, dissolved, entrapped, encapsulated, or attached to polymers [21]. Among these polymers, polyethylene glycol

(PEG), a particulate drug carrier modifier, has been extensively used to decrease toxicity and extend the circulation time and controlled release of drugs [22]. AuNPs that are surface modified with PEG are good carriers for both imaging and therapeutic purposes [17]. In this study, we formulated AuNPs using PEG due to its biocompatibility and high drug-loading capability. Furthermore, we selected anthocyanins for encapsulation in PEGylated AuNPs [22].

Anthocyanins, which are polyphenolic flavonoids found in fruits, flowers, and leaves of plants, have been shown to beneficially affect memory and cognition [23, 24]. Our group previously demonstrated the neuroprotective effects of anthocyanins extracted from Korean black soybeans in vitro against kianic acid-induced excitotoxicity in hippcampal neuronal HT22 cells and in vivo against apoptosis, neurodegeneration, and neuroinflammation in post-natal rat brains of ethanol-treated pups and adult rat brains of D-galactose- and lipopolysaccharide-treated rodents [25–28]. These findings demonstrated that anthocyanins are beneficial for treating neurodegenerative disorders. Furthermore, our lab recently investigated the ability of anthocyanins to mitigate the neurodegenerative effects of $A\beta_{1-42}$ both in vitro and in vivo Aβ models of AD [29]. Curcumin, a natural polyphenol, was encapsulated in PEGylated cobalt ferrite to improve its biocompatibility and delivery [30]. Akhtar et al. reported that the bioavailability of orally delivered curcumin-loaded chitosan nanoparticles was improved in the plasma and red blood cells [31]. Another study reported the covalent conjugation of curcumin to AuNPs that were functionalized using folic acid-conjugated PEG [32]. Curcumin has also been conjugated to polyvinyl pyrrolidone-capped AuNPs [33].

Based on these studies, we selected polyphenolic flavonoid anthocyanins for conjugation to PEG-AuNPs. Next, we investigated the ability of these particles to mitigate $A\beta_{1-42}$-induced memory and synaptic deficits and neurodegeneration in an $A\beta_{1-42}$ mouse model of AD.

## Materials and Methods

### Chemicals

$A\beta_{1-42}$ and AuNPs of 5 nm with PEG in aqueous suspension were purchased from Sigma-Aldrich (Saint Louis, MO, USA). The PEG-AuNPs were stored at 4 °C in order to prevent aggregation. Anthocyanins were extracted from black beans as previously described [26].

### 3-[4,5-Dimethylthiazol-2-yl]-2,5-diphenyltetrazolium bromide Assay

Colorimetric 3-[4,5-dimethylthiazol-2-yl]-2,5-diphenyltetrazolium bromide (MTT) assays were employed to measure the viability of immortalized hippocampal HT22 neuronal cells treated with different concentrations of PEG-AuNPs. The HT22 neuronal cells were seeded into 96-well plates ($1 \times 10^5$ cells/well) in 200 μl of Dulbecco's modified Eagle's medium (DMEM). After 48 h of incubation, the HT22 neuronal cells were treated with PEG-AuNPs and incubated for 12 h. At the end of the treatment period, MTT (5 mg/ml in phosphate-buffered saline (PBS)) was added to each well, and the plates were incubated for 4 h at 37 °C. Formazan dissolved in dimethyl sulfoxide (DMSO) was added to the wells, and the plates were agitated for 10 to 20 min on a shaker. The absorbance was then measured at 550–570 nm (L1) and 620–650 nm (L2) using a scanning microplate reader. The L2 absorbance measures cell debris and well imperfections. The corrected absorbance ($A = L1 - L2$) of each well was used to calculate the percentage of cell survival as ×100 absorbance of the treated wells/absorbance of control wells.

### ApoTox-Glo™ Triplex Assay

The ApoTox-Glo™ Triplex assay (Promega Corporation, 2800 Woods Hollow Road Madison, WI 53711-5399, USA) was performed to assess cell toxicity, viability, and caspase$^{3/7}$ activation with a single 96-well assay. HT22 neuronal cells ($2 \times 10^4$) were cultured in 96-well plates containing a final volume of 200 μl of DMEM with 1 % penicillin/streptomycin and 10 % fetal bovine serum (FBS) solution. The cells were cultured at 37 °C in humidified air containing 5 % carbon dioxide. After 48 h of incubation, the cells were treated with gradually increasing concentrations (0.5, 1, 5, and 10 % *v*/*v*) of PEG-AuNPs. For the assay, 20 μl of the viability/cytotoxicity reagent was added to all wells and briefly mixed via orbital shaking (500 rpm for 30 s), followed by incubation for 1 h at 37 °C. The reagent contained both the glycyl-phenylalanyl-amino-fluorocoumarin (GF-AFC) and bis-alanyl-alanyl-phenylalanyl-rhodamine 110 (bis-AAF-R110) substrates. The fluorescence was measured at two wavelengths, 400/505 and 485/520 nm, to assess the viability and the cytotoxicity, respectively. The GF-AFC substrate enters live cells, where it is cleaved by proteases within the cells to release AFC. The bis-AAF-R110 is cleaved by proteases in dead cells rather than live cells to release R110. The live cell activity was measured using a fluorogenic substrate of the cell-permeating GF-AFC. A second fluorogenic compound, bis-AAF-R110, a cell-impermeable peptide, was used to measure the dead cell proteases, which are released from dead cells that have lost membrane integrity.

The second part of the assay employed a luminogenic caspase$^{3/7}$ substrate, which contains the tetrapeptide sequence DEVD, to measure the caspase$^{3/7}$ activity. The caspase-Glo reagent was added (100 μl) to all wells and briefly mixed via orbital shaking (500 rpm for 30 s). After incubation for 30 min

at room temperature, the luminescence was measured to assess caspase$^{3/7}$ activation.

### Preparation and Characterization of Anthocyanin-Loaded PEG-AuNPs

PEG-5000-coated AuNPs in an aqueous suspension were purchased from Sigma-Aldrich (Saint Louis, MO, USA). The AuNPs were stored at 4 °C to prevent aggregation. We used a previously described process with some modifications to conjugate anthocyanins to the PEG-AuNPs [32]. Briefly, 50 mg of anthocyanins was dissolved in 25 ml acetone, and this solution was added to 100 ml of PEG-AuNPs while stirring. This mixture was then stirred for 3 h at 60 °C and then cooled to room temperature. The solution was then centrifuged at 4000 rpm to remove unattached anthocyanins. This procedure was performed three times to ensure that no free anthocyanin molecules remained in the final conjugate. The final solution was analyzed with transmission electron microscopy (TEM) (Tecnai-12, 120 kV). Part of this solution was freeze-dried to obtain a powder, which was used for zeta potential and Fourier transform infrared spectroscopy (FTIR) analyses. Similarly, a coumarin-6 fluorescence dye was conjugated to the PEG-AuNPs to analyze the PEG-AuNP uptake in a mouse bEnd.3 cell line (ATCC, USA), which served as an in vitro BBB model.

### Characterization

The free anthocyanins, PEG-coated AuNPs and anthocyanin-loaded PEG-AuNPs, were characterized by FTIR (SMART-APEXII ULTRA FTIR, PerkinElmer) and TEM. For the TEM (TEM, Tecnai-12, 120 kV) analysis, the anthocyanin-loaded PEG-AuNP samples were dropped on the slides and stained with an aqueous solution of 10 % uranyl acetate. Furthermore, the surface charge of the anthocyanin-loaded PEG-AuNPs was characterized based on the zeta potential using electrophoretic light scattering (ELS-Z; Otsuka Electronics Co., Osaka, Japan) at a scattering angle of 20°. The average particle sizes of the anthocyanin-loaded PEG-AuNPs were determined based on the light-scattering method (DLS-8000; Otsuka Electronics Co., Osaka, Japan).

### In Vitro Uptake of PEG-AuNPs

The uptake of coumarin-loaded PEG-AuNPs (C-6-PEG-AuNPs) was studied in a mouse bEnd.3 cell line (ATCC, USA), which served as an in vitro BBB model, using confocal laser scanning microscopy (CLSM). For the CLSM (Fluoview FV 1000, Olympus, Japan) analysis, a freshly prepared C-6-PEG-AuNP suspension at a concentration of 0.1 mg/ml was mixed with cell culture medium and added to cells that were pre-cultured in 4-well cover glass chambers, and the cells were then incubated for 4 h. However, to the control group cells (cells not treated with C-6-PEG-AuNP suspension), only the culture medium was changed and applied the same condition. Following incubation, the cells were washed three times with PBS, fixed with 4 % paraformaldehyde, and again washed with PBS. The slides were mounted with 4′,6-diamidino-2-phenylindole (DAPI) and ProLong Antifade Reagent (Molecular Probe, Eugene, OR, USA). The representative images were captured using fluorescein isothiocyanate (FITC), DAPI, and bright field filter via CLSM (FV 1000, Olympus, Japan).

### Animals and Drug Administration

Male mice C57BL/6N from Samtako Bio (South Korea) aged 8–10 weeks (25-g average body weight) were housed under a 12/12-h light/dark cycle at 23 °C and 10 % humidity. The mice were provided free access to water and food. All methods complied with the guidelines (approval ID 125) of the animal ethics committee (IACUC) of the Division of Applied Life Sciences, Department of Biology at Gyeongsang National University, South Korea. The experimental animals were divided into the following four groups ($n$ = 15 per group): mice injected (1) with 0.9 % saline as the vehicle (control) (C), (2) $A\beta_{1–42}$ ($A\beta_{1–42}$), (3) $A\beta_{1–42}$ + anthocyanins (12 μg/g/day for 14 days) ($A\beta_{1–42}$ + An), and (4) $A\beta_{1–42}$ + PEG-AuNPs + anthocyanins (12 μg/g/day for 14 days) ($A\beta_{1–42}$ + AuNPs + An).

A 1 mg/ml stock solution of human $A\beta_{1–42}$ peptide was prepared in sterile saline. The peptide was incubated at 37 °C for 4 days to form aggregates. The aggregated $A\beta_{1–42}$ peptide or vehicle (0.9 % NaCl, 3 μl/5 min/mouse) was intracerebroventricularly (i.c.v.) injected using a Hamilton microsyringe at stereotaxic coordinates from the bregma (anteroposterior (AP) 0.2 mm, mediolateral (ML) = 1 mm, and dorsoventral (DV) = 2.4 mm) under anesthesia in combination with Rompun (0.05 ml/100 g body weight) and Zoletil (0.1 ml/100 g body weight). During the stereotaxic procedure, the body temperature of the animals was controlled to prevent anesthetic-induced hypothermia, which triggers tau hyperphosphorylation [34].

Seven days after $A\beta_{1–42}$ injection, anthocyanins and anthocyanin-loaded PEG-AuNPs (12 μg/g/day for 14 days) were injected into the tail vein for 14 days. We calculated the amount of anthocyanins (12 μg/g/day for 14 days) in the anthocyanin-loaded PEG-AuNPs in the primary and fundamental studies according to the previously described methods by Shah et al. [35]. For muscular tonus relaxation, the mice were anesthetized via isoflurane (5 %) inhalation. Care was taken to maintain the body temperature of the animals during anesthesia because hypothermia increases the phosphorylation of tau protein [34].

### Behavioral Studies

A Morris water maze (MWM) and a Y-maze task were used to analyze mouse behavior ($n$ = 15/group) after completion of the treatment.

### MWM Test

The experimental apparatus consisted of a circular water tank (100 cm in diameter, 40 cm in height) containing water (23 ± 1 °C) at a depth of 15.5 cm, which was made opaque by adding white ink. A transparent platform (10 cm in diameter, 20 cm in height) was submerged 1 cm below the surface of the water and maintained in the center of one quadrant. The pool was located in a test room, which contained various prominent visual cues. Each mouse received four training periods per day for five consecutive days. The latency to escape from the water (to find the submerged escape platform) was calculated for each trial. On day 7, the probe test was performed by removing the hidden platform and allowing each mouse to swim freely for 60 s. The time that the mouse spent swimming in the target quadrant and the number of platform crossings (where the platform was located during the hidden platform training session) were measured. All data were recorded using a video-tracking software (SMART, Panlab Harvard Apparatus, Bioscience Company, USA).

### Y-Maze Test

The maze was constructed of black-painted wood. Each arm of the maze was 50 cm long, 20 cm high, 10 cm wide at the bottom, and 10 cm wide at the top. The Y-maze apparatus was used in a separate illuminating room. Each mouse was placed at the center of the apparatus and allowed to move freely through the maze for three 8-min sessions. The series of arm entries was noted. A spontaneous alteration was defined as the successive entry of the mouse into the three arms in overlapping triplet sets. The alteration behavior (%) was calculated as follows: [successive triplet sets (entries into three different arms consecutively)/total number of arm entries − 2] × 100. Higher percentages of spontaneous alteration behavior were considered to indicate enhanced cognitive performance. Upon completion of the behavioral analysis, the animals were killed for biochemical and immunohistochemical analyses.

### Western Blotting

The mice (10 mice/group) were sacrificed after the behavioral analysis for the western blot analysis. The brains were rapidly removed and the hippocampus regions were dissected and frozen on dry ice. The hippocampus was homogenized in 0.2 M PBS containing protease inhibitor. A Bio-Rad Protein Assay Kit (Bio-Rad Laboratories, CA, USA) was used to measure the protein concentration of homogenates. Equal amounts of total protein (15–30 μg) were loaded on 4–12 % Bolt™ Mini Gels and separated with electrophoresis in MES SDS running buffer ×1 (Novex, Life Technologies, Kiryat Shmona, Israel) using the same conditions. Pre-stained protein ladders (GangNam stain™ iNtRON Biotechnology) covering broad ranges of molecular weights (10–245 kDa) were used as molecular size controls. Skim milk (5 %) was used to block the membranes and reduce non-specific binding. The membranes were incubated with primary antibodies (1:1000 dilutions) overnight at 4 °C. Horseradish peroxidase-conjugated secondary antibody was used to detect the protein. Proteins were detected using ECL detection reagents according to the manufacturer's instructions (Amersham Pharmecia Biotech, Uppsala, Sweden). The X-ray films were scanned. The optical densities of bands on X-ray films were analyzed via densitometry using a computer-based Sigma Gel program version 1.0 (SPSS, Chicago, IL, USA).

### Primary Antibodies Used in Western Blot

The following primary antibodies were used: anti-Aβ, anti-beta-site amyloid precursor protein cleaving enzyme 1 (BACE-1), anti-synaptosomal associated protein 23 (SNAP23), anti-synaptophysin, anti-phospho-AMPARs (GluR1) Ser845), anti-phosphorylated phosphatidylinositol 3-kinase (p-PI3K), anti-p-Akt serine (Ser) 473, anti-phosphorylated glycogen synthase kinase-3 β (p-GSK3β) Ser 9, anti-p-Tau at Ser 413 and Ser 404, anti-post-synaptic density (PSD95), anti-caspase-3, anti-cytochrome c (Cyt c), anti-Bax, anti-Bcl2, anti-poly (ADP-ribose) polymerase-1 (PARP-1), and anti-β-actin from Santa Cruz Biotechnology, Dallas, TX, USA; anti-phosphorylated cAMP response element-binding protein (p-CREB) (Ser 133) and anti-caspase-9 from Cell Signaling Technology, Beverly, MA, USA; and anti-amyloid precursor protein (APP) from Millipore (Billerica, MA, USA).

### Tissue Collection and Sample Preparation

After the behavioral analysis, the mice (five mice/group) were transcardially perfused with ×1 PBS, followed by 4 % ice-cold paraformaldehyde. The brains were incubated in paraformaldehyde (4 %) overnight at 4 °C and then transferred to 20 % sucrose for 72 h. The brains were transferred to O.C.T. compound medium for freezing and then sectioned into 14-μm-thick sections in the coronal plane using a CM 3050C cryostat. The sections were thaw mounted on probe-on positively charge slides.

### Confocal Microscopy

Confocal microscopy was performed according to what we described previously [36–39]. Briefly, slide with tissues were washed twice for 10 min in 0.01 M PBS. The slides were then incubated for 90 min in blocking solution containing normal goat/bovine serum and 0.3 % Triton X-100 in PBS. The primary antibodies (mouse monoclonal Aβ) were diluted 1:100 in PBS and incubated overnight at 4 °C. On the next day, the slides were incubated in secondary antibodies (TRITC-labeled) diluted 1:50 in PBS for 2 h at room temperature. The slides were washed twice with PBS for 5 min. The slides were mounted with DAPI and ProLong Antifade Reagent. The staining patterns of the immunofluorescence were examined using CLSM (Fluoview FV 1000, Olympus, Japan).

### Immunohistochemical Nissl Staining

Immunohistochemical Nissl staining was performed as we described previously [40, 41].

### Immunohistochemical Fluoro-Jade B Staining

Fluoro-Jade B (FJB), a marker of neuronal degeneration, was used to stain brain cells; the procedure was performed with some modification as previously described [42] and according to the manufacturer's protocols (Millipore, USA, catalog no. AG310, lot no. 2159662). The slides of the brain tissue were air-dried for at least 4 h. The slides were washed twice for 5 min. Following washing, the slides were immersed in a 1 % sodium hydroxide and 80 % ethanol solution for 5 min and then in 70 % alcohol for 2 min, followed by 2 min in distilled water. Next, the slides were transferred to a solution of 0.06 % potassium permanganate for 10 min over a slow shaker, rinsed with distilled water, and then immersed in a 0.1 % acetic acid and 0.01 % Fluoro-Jade B solution for 20 min. The slides were then rinsed with distilled water and dried for at least 10 min. The slides were mounted with propidium iodide (PI) and glass coverslips using DPX non-fluorescent mounting medium. The representative images were captured using an FITC filter via CLSM (FV 1000, Olympus, Japan). The number of cells with FJB-positive nuclei was analyzed and counted using ImageJ program analysis.

### Statistics

The western blot bands were scanned and analyzed through densitometry using the Sigma Gel system (SPSS Inc., Chicago, IL, USA). The density values were expressed as the means ± standard error mean (SEM). The ImageJ software was used for immunohistological quantitative analysis. One-way analysis of variance (ANOVA) followed by a two-tailed independent Student's *t* test and Tukey's multiple comparison test were used for comparisons among the treated groups and the control. The calculations and graphs were made through Prism 5 software (GraphPad Software Inc., San Diego, CA, USA). *p* Values less than 0.05 were considered to be statistically significant. An asterisk indicates the significant differences from the vehicle-treated control group, while phi sign and pound sign indicate the significant differences from the $A\beta_{1-42}$-treated groups ($^{*}p < 0.05$, $^{**}p < 0.01$, and $^{***}p < 0.001$; $^{\Phi}p < 0.05$, $^{\Phi\Phi}p < 0.01$, and $^{\Phi\Phi\Phi}p < 0.001$; and $^{\#}p < 0.05$, $^{\#\#}p < 0.01$, and $^{\#\#\#}p < 0.001$).

## Results

### In Vitro Cytotoxicity of PEG-AuNPs

Several previous studies have reported that AuNPs are minimally toxic, and Bouzas et al. (2013) recently showed that PEG-AuNPs are not cytotoxic [43]. We used MTT and ApoTox-Glo™ Triplex assays to assess the toxicity of PEG-AuNPs in the HT22 cells. We used increasing concentrations (0.5, 1, 5, and 10 % *v*/*v*) of PEG-AuNPs to measure cell viability. The results of the MTT assay showed that the PEG-AuNPs did not significantly affect cell viability, indicating that they are not toxic (Fig. 1a).

Next, we performed an ApoTox-Glo™ Triplex assay to analyze the cell viability, cytotoxicity, and apoptosis (using the apoptotic marker caspase$^{3/7}$) in HT22 cells. Similar to the results of the MTT assay, the results of the ApoTox-Glo™ Triplex assay showed that the cell viability, cytotoxicity, and apoptosis did not significantly differ among cells treated with various concentrations of PEG-AuNPs (0.5, 1, 5, and 10 % *v*/*v*) (Fig. 1b), again indicating that the PEG-AuNPs are non-toxic.

### Anthocyanin-PEG-AuNP Conjugation and Characterization

After analyzing the toxicity of the PEG-AuNPs, we prepared anthocyanin-loaded PEG-AuNPs by conjugating anthocyanins to PEG, which was attached to the surface of the gold via an Au-S bond. The conjugation of anthocyanins with the PEG-AuNPs was confirmed by FTIR spectroscopy. Infrared absorption spectra were obtained from 500 to 3500 $cm^{-1}$ to identify the active groups of organic and inorganic compounds and to compare their changes. Figure 2a shows the FTIR spectra of (i) anthocyanins, (ii) PEG-AuNPs, and (iii) anthocyanin-loaded PEG-AuNPs. Spectrum (i) shows the structure of the anthocyanins, which was characterized by a benzene ring (1550 $cm^{-1}$), a free OH group (3514 $cm^{-1}$), and a methyl (2845 $cm^{-1}$) group. Spectrum (ii) illustrates the functionalization of PEG with gold in the form of C = O from

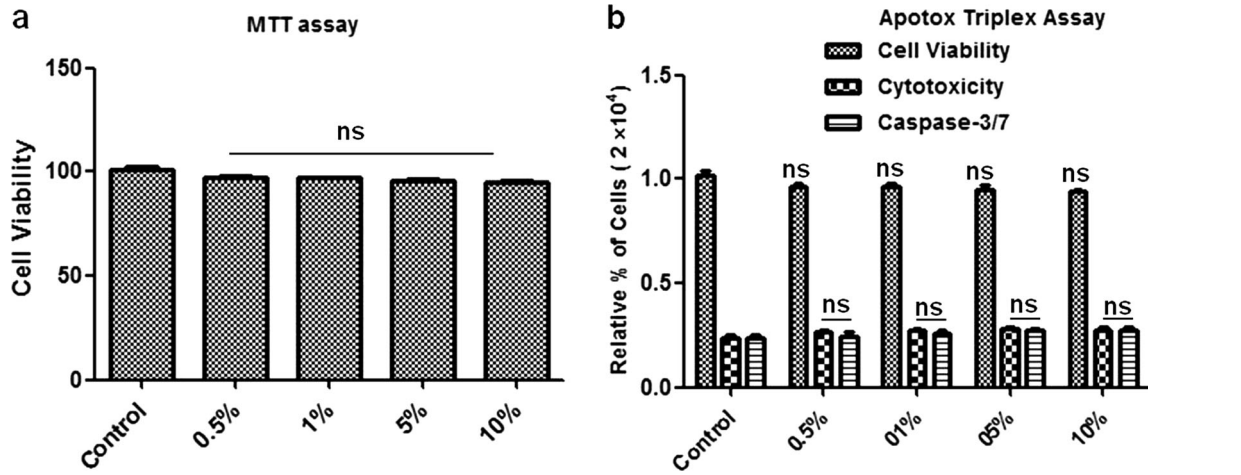


**Fig. 1** In vitro cytotoxicity of PEG-AuNPs. **a** MTT assays using increasing concentrations of PEG-AuNPs (0.5, 1, 5, and 10 % *v*/*v*) showed no significant changes in the viability of HT22 cells. **b** The ApoTox-Glo™ assay showed no significant differences in the cell viability, cytotoxicity, and apoptosis in the HT22 cells in response to increasing concentrations (0.5, 1, 5, and 10 % *v*/*v*) of PEG-AuNPs. $N = 3$ experiments each, *ns* = not significant

1660 to 1628 $cm^{-1}$. The anthocyanin-loaded PEG-AuNP spectrum shows all peaks belonging to the AuNPs and anthocyanins. The anthocyanins are attached to the PEG-AuNPs via intermolecular hydrogen to the hydroxyl group, which is indicated in the spectrum as stretching from 3435 to 3420 $cm^{-1}$.

Next, we observed the morphology and size distribution of the anthocyanin-loaded PEG-AuNPs via TEM. The TEM result showed that the anthocyanin-loaded PEG-AuNPs were highly spherical, well dispersed, and uniform (Fig. 2b). Subsequently, the mean particle size of the anthocyanin-loaded PEG-AuNPs was analyzed via the light-scattering method (DLS). The mean particle size of the anthocyanin-loaded PEG-AuNPs was found to be approximately 135 ± 5 nm (Fig. 2c). We also measured the zeta potential because the charge of the nanoparticles is a critical parameter for delivery to the brain. The anthocyanin-loaded PEG-AuNPs showed negative zeta potentials (−11.5 ± 2) (Fig. 2d). The conjugation of anthocyanins with PEG-AuNPs did significantly change the zeta potential. Figure 2e shows a possible schematic illustration of the conjugation of anthocyanins with PEG-AuNPs. As shown in the figure, anthocyanins are attached to the hydroxyl groups via intermolecular hydrogen bonds, which shift the O–H stretching from 3435 to 3420 $cm^{-1}$ in the FTIR spectra (Fig. 2a).

### Cellular Uptake of PEG-AuNPs

The uptake and cytoplasmic localization of the PEG-AuNPs were investigated in the bEnd.3 cell line using CLSM. Figure 3 shows the uptake and intracellular retention of C-6-PEG-AuNPs as revealed by CLSM. As shown in Fig. 3, the bEnd.3 cells internalized C-6-PEG-AuNPs, as indicated by the intensity of FITC green fluorescence as compared to the control cell group, which corresponds to the cytoplasmic localization of C-6-PEG-AuNPs.

### Anthocyanin-Loaded PEG-AuNP Treatment Alleviated $A\beta_{1–42}$-Induced Memory Deficits

To evaluate the neuroprotective effects (i.e., ability to ameliorate $A\beta_{1–42}$ infusion-induced memory impairment) of the anthocyanin-loaded PEG-AuNPs and free anthocyanins, we performed MWM and Y-maze tests. The MWM was used to observe the learning ability of the mice ($n$ = 15/group) via training with a hidden platform. We noticed that $A\beta_{1–42}$-infused mice required more time to reach the hidden platform, while the latency times of the mice treated with free anthocyanins and anthocyanin-loaded PEG-AuNPs (12 μg/g/day for 14 days) were shorter (Fig. 4a). We performed a probe test 1 day after a training session. We observed that $A\beta_{1–42}$-injected mice crossed the platform less frequently and spent less time in the target quadrant, which demonstrated $A\beta_{1–42}$-induced memory impairment. Anthocyanin and anthocyanin-loaded PEG-AuNP administration reversed this $A\beta_{1–42}$-induced memory deficit and significantly increased the number of platform crossings and time spent in the target quadrant during the probe test ($p < 0.001$; Fig. 4b, c).

Furthermore, we observed that administration of $A\beta_{1–42}$ significantly reduced the percentage of spontaneous alteration behavior compared with the control mice, suggesting that $A\beta_{1–42}$ induced memory dysfunction. Anthocyanins and anthocyanin-loaded PEG-AuNPs significantly increased the spontaneous alteration behavior in the $A\beta_{1–42}$-injected mice compared with mice injected with only $A\beta_{1–42}$ ($p < 0.001$; Fig. 4d).

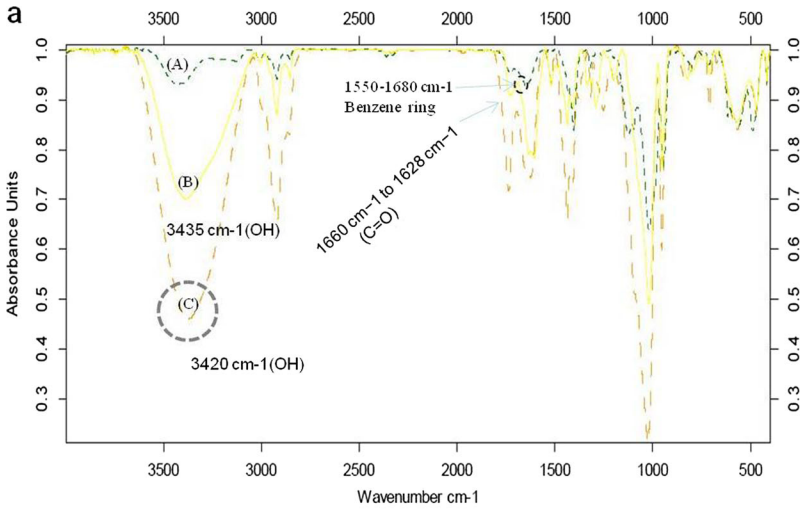


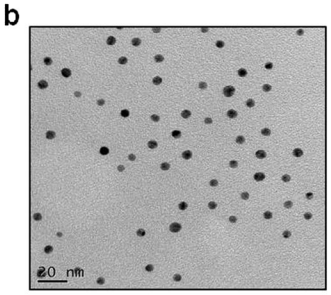


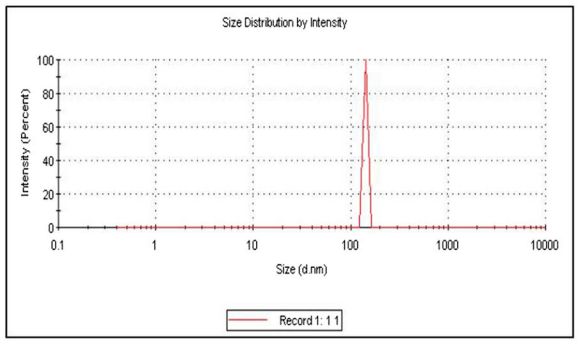


d

| Nanoparticles | Particle size(nm) | Zeta potential(mV) |
|---|---|---|
| PEG-AuNPs + An | 135 ± 5 | -11.5 ± 2 |

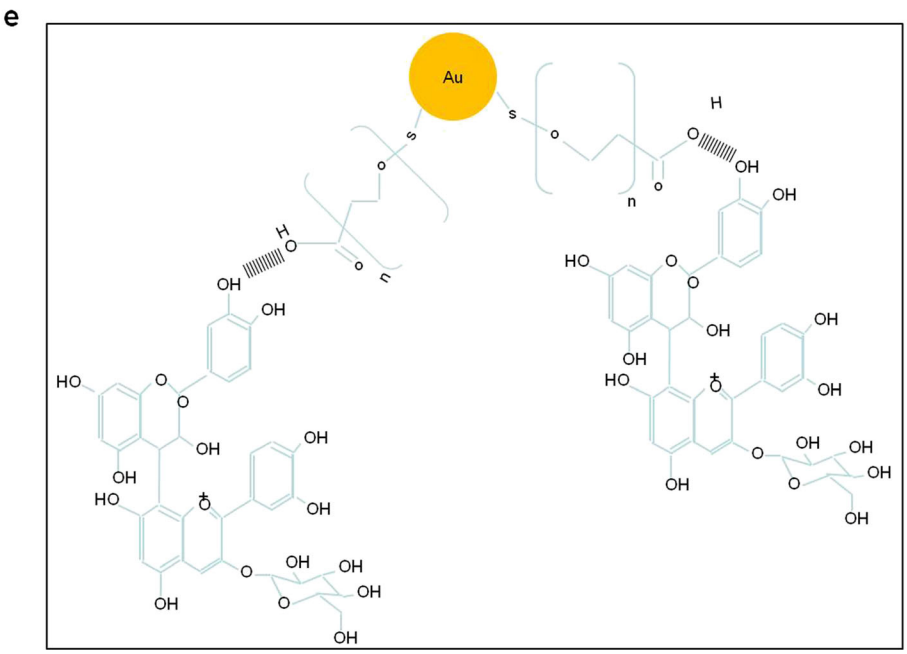


**Fig. 2** Anthocyanin-PEG-AuNP conjugation and characterization. **a** The conjugation of anthocyanins into PEG-AuNPs was confirmed by FTIR spectroscopy. **b** Morphology and size distributions of the anthocyanin-loaded PEG-AuNPs via TEM. *Scale bar* = 20 nm. **c** The mean particle size of anthocyanin-loaded PEG-AuNPs was analyzed using the DLS method. **d** The zeta potential of the anthocyanin-loaded PEG-AuNPs. **e** Schematic illustration of the conjugation of anthocyanins with PEG-AuNPs

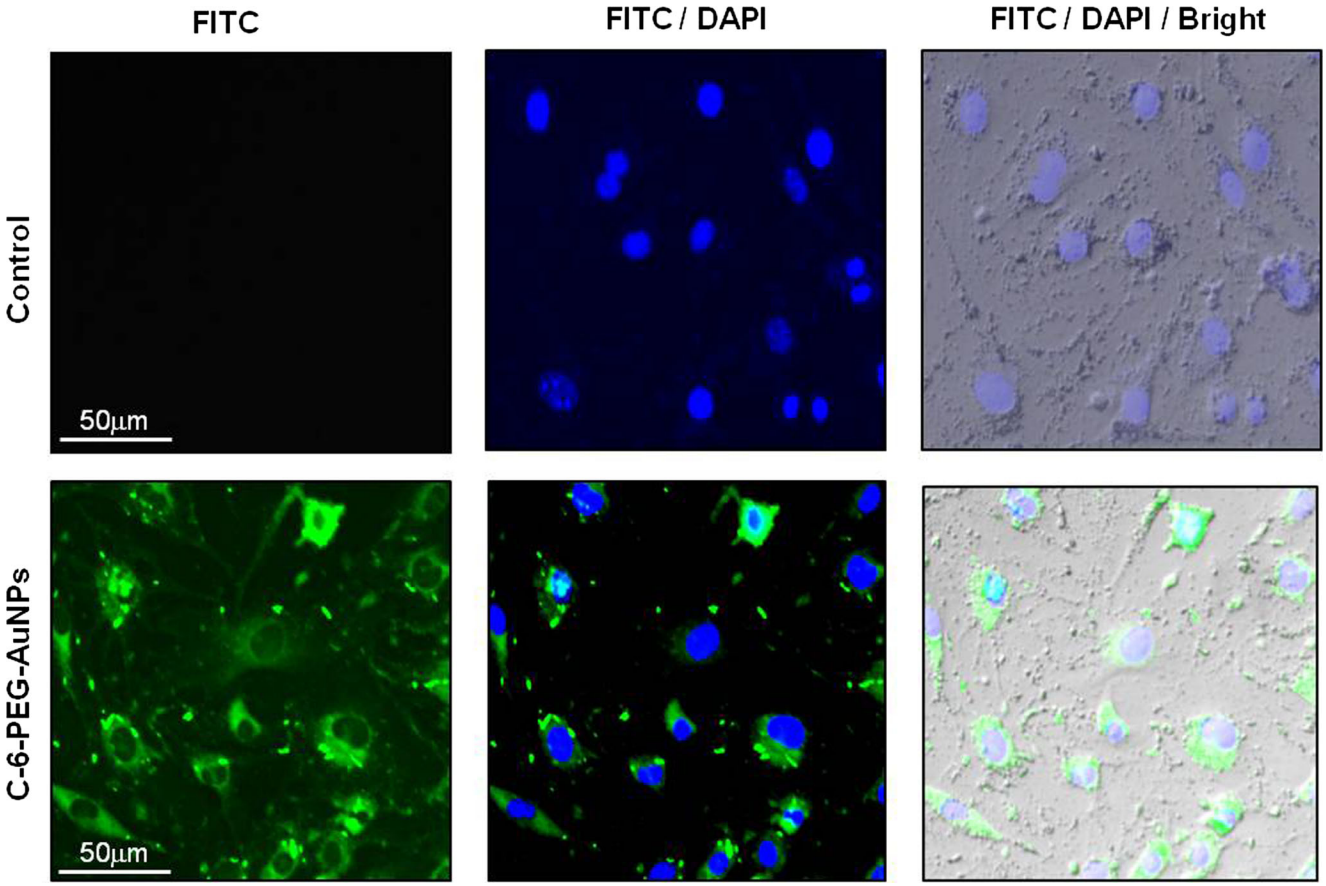


**Fig. 3** Cellular uptake of PEG-AuNPs. Confocal microscopy shows that C-6-PEG-AuNPs were taken up by mouse brain bEnd.3 cells. Magnification ×40, *scale bar* = 50 μm

### Anthocyanin-Loaded PEG-AuNPs Reduced the Levels of Aβ, BACE-1, and APP in $A\beta_{1–42}$-Treated Mice

The expression level of Aβ after $A\beta_{1–42}$ infusion was analyzed using western blot. The results showed that level of Aβ increased in the $A\beta_{1–42}$-injected mice compared with the control mice. The anthocyanins and anthocyanin-loaded PEG-AuNPs (12 μg/g/day for 14 days) significantly reduced the level of Aβ in the $A\beta_{1–42}$-injected mice compared with the mice injected only with $A\beta_{1–42}$ (Fig. 5a).

The immunofluorescence results showed that the reactivity of Aβ in the cortex and CA1 region of hippocampus in the $A\beta_{1–42}$-injected mice increased compared with the control group. The administration of anthocyanin-loaded PEG-AuNPs to the $A\beta_{1–42}$-injected group significantly reduced the Aβ immunofluorescence reactivity in the cortex and CA1 region of hippocampus compared with the $A\beta_{1–42}$-injected group (Fig. 5b).

Recent studies have demonstrated that $A\beta_{1–42}$ exposure upregulates BACE-1 expression [44–46]. Similarly, our western blot results also showed that BACE-1 and APP expressions were increased in the $A\beta_{1–42}$-injected mice compared with the control mice. Treatment with anthocyanins and anthocyanin-loaded PEG-AuNPs (12 μg/g/day for 14 days) significantly decreased BACE-1 and APP expressions compared with the $A\beta_{1–42}$-injected group (Fig. 5a).

### Anthocyanin-Loaded PEG-AuNPs Mitigated $A\beta_{1–42}$-Induced Synaptic Dysfunction

The western blot analysis showed reduced levels of synaptophysin, PSD95, and SNAP-23 in the $A\beta_{1–42}$-injected mice compared with the control mice. The administration of free anthocyanins and anthocyanin-loaded PEG-AuNPs (12 μg/g/day for 14 days) mitigated the effect of $A\beta_{1–42}$ and significantly increased the expression levels of synaptophysin, PSD95, and SNAP23 (Fig. 6).

The $A\beta_{1–42}$-triggered reduction of α-amino-3-hydroxy-5-methylisoxazole-4-propionic acid (AMPA) receptor (AMPAR) is responsible for synaptic impairment; notably, the phosphorylation of AMPA receptor 1 (GluR1) at Ser 845 plays a pivotal role in the trafficking of post-synaptic glutamate receptors [47]. Therefore, we analyzed the phosphorylation of GluR1 at Ser 845. The western blot results showed that the phosphorylation of GluR1 at Ser 845 decreased in the $A\beta_{1–42}$-injected mice compared with the control mice.

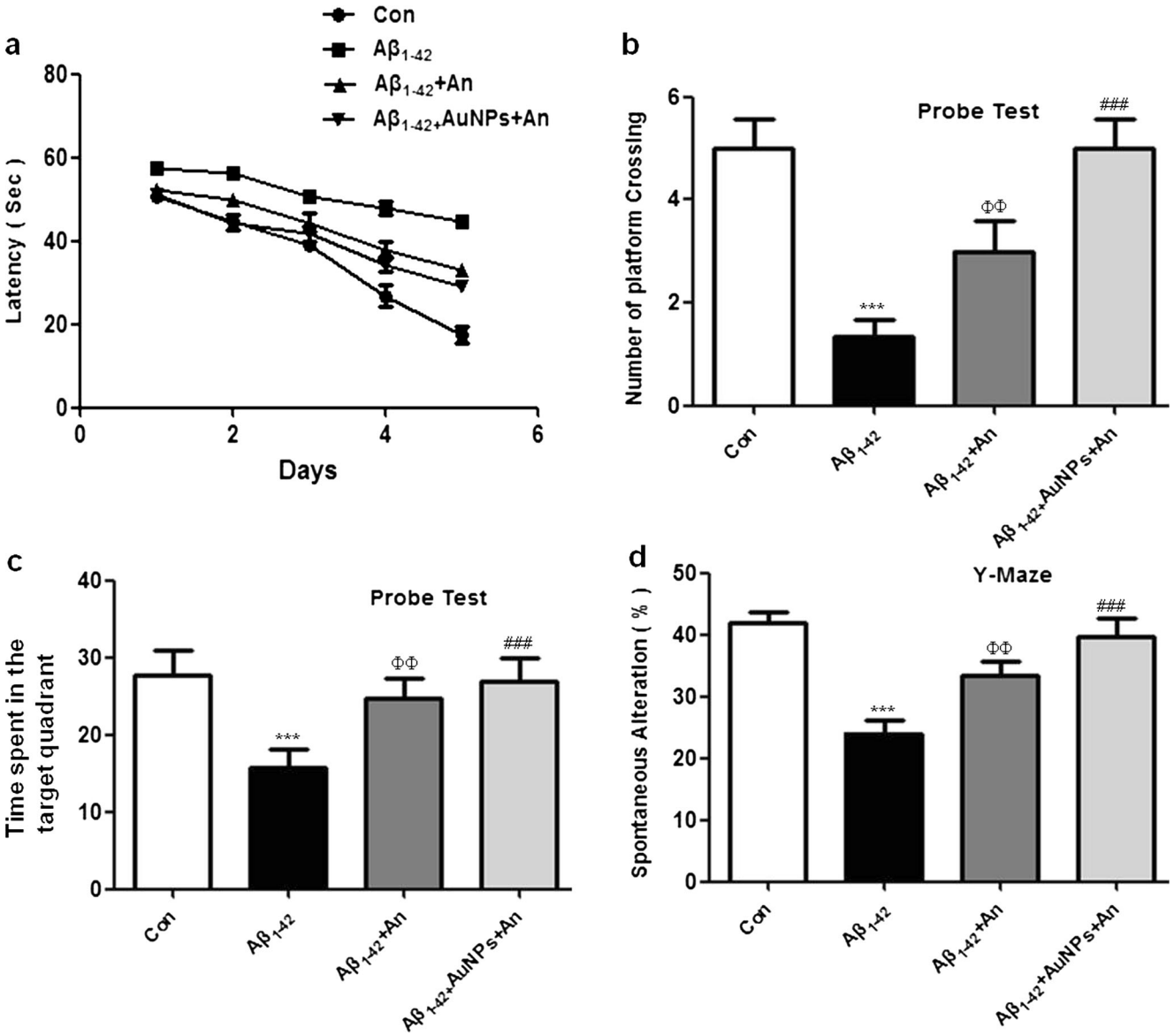


**Fig. 4** Anthocyanin-loaded PEG-AuNP treatment alleviated $A\beta_{1–42}$-induced memory deficits. Fifteen mice per group were used for the behavioral analysis. **a** The histogram represents the mean escape latency (sec) during the training session. **b** The histogram represents the number of platform crossings during the probe test. **c** The histogram represents the time spent in the target quadrant during the probe test. **d** The histogram represents the spontaneous alteration behavior percentage in the Y-maze test. The *graphs* were expressed as the means ± SEM ($n$ = 15 mice/group). The *asterisk* indicates the significant differences compared to the vehicle-treated control group, while the *phi sign* and *pound sign* indicate the significant differences compared to the $A\beta_{1–42}$-injected groups. Significance at $^{***}p < 0.001$, $^{\Phi\Phi}p < 0.01$, and $^{\#\#\#}p < 0.001$

Anthocyanins and anthocyanin-loaded PEG-AuNPs (12 μg/g/day for 14 days) significantly increased the phosphorylation of GluR1 at Ser 845 in the $A\beta_{1–42}$-injected mice (Fig. 6).

Furthermore, the immunoblot results revealed decreased p-CREB (Ser 133) expression in the $A\beta_{1–42}$-injected mice compared with the control mice. Anthocyanins and anthocyanin-loaded PEG-AuNPs (12 μg/g/day for 14 days) administration significantly increased the expression level of p-CREB (Ser 133) in the $A\beta_{1–42}$-injected mice compared with the mice only injected with $A\beta_{1–42}$ (Fig. 6).

## Anthocyanin-Loaded PEG-AuNPs Regulated $A\beta_{1–42}$-Induced Dysregulated p-PI3-K/p-Akt/p-GSK-3β Signaling and Prevented Tau Phosphorylation at Ser 413 and 404

The abnormal p-PI3-K/Akt/GSK3β signaling pathway, which affects tau hyperphosphorylation and neurodegeneration, has been implicated in the Aβ mouse model of AD [48]. Our immunoblotting results revealed that the p-PI3K and p-Akt (also known as protein kinase B) at Ser473 were significantly

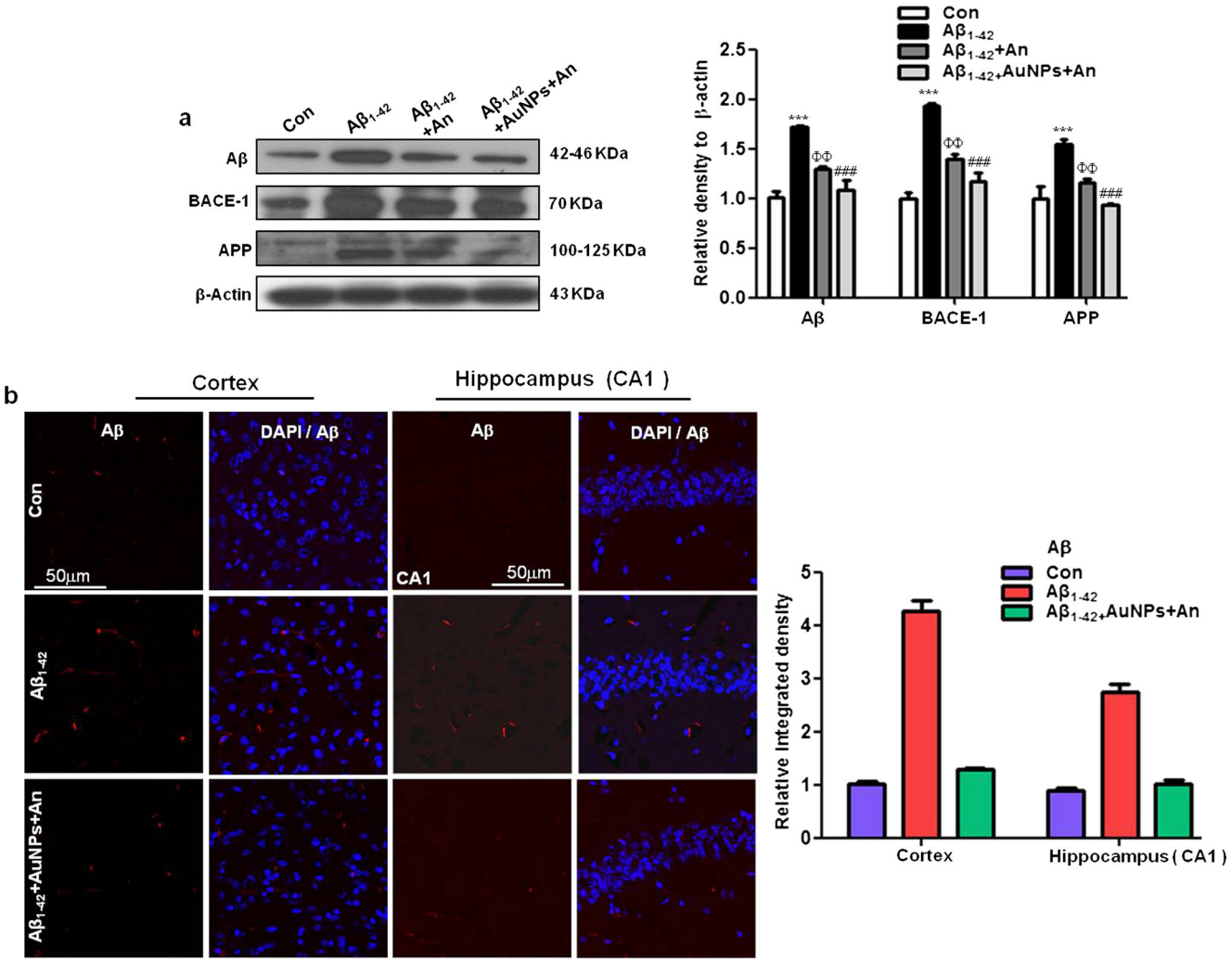


**Fig. 5** Anthocyanin-loaded PEG-AuNPs reduced the levels of Aβ, BACE-1, and APP in $A\beta_{1-42}$-treated mice. **a** Western blot bands of Aβ, BACE-1, and APP in the hippocampus of mice were quantified using the Sigma Gel software, and the differences are represented by a histogram. β-actin was used as a loading control. The density values are expressed in arbitrary units (A.U.) as the mean ± SEM for the respective indicated protein ($n$ = 10 mice/group). The *asterisk* indicates the significant differences compared to the vehicle-treated control group, while the *phi sign* and *pound sign* indicate the significant differences compared to the $A\beta_{1-42}$-injected groups. Significance at $^{***}p < 0.001$, $^{\Phi\Phi}p < 0.01$, and $^{\#\#\#}p < 0.001$. **b** Immunofluorescence images represent the immunoreactivity of Aβ in the cortex and hippocampus of the experimental mice. Magnification ×40, *scale bar* = 50 μm. The data are expressed as the means ± SEM. The *asterisk* indicates the significant differences compared to the vehicle-treated control group, and the *pound sign* indicates the significant differences compared to the $A\beta_{1-42}$-injected groups. Significance at $^{***}p < 0.001$ and $^{\#\#\#}p < 0.001$

reduced in the $A\beta_{1-42}$-injected mice compared with the control mice. The administration of free anthocyanins and anthocyanin-loaded PEG-AuNPs (12 μg/g/day for 14 days) increased phosphorylation and significantly elevated the levels of p-PI3K and p-Akt at Ser 473 in mice injected with $A\beta_{1-42}$ compared with mice injected with only $A\beta_{1-42}$ (Fig. 7).

The phosphorylation of GSK-3β at Ser9 (p-GSK3β at Ser9) reduced the activity of GSK-3β by activating p-Akt at Ser 473 [49]. In parallel with the p-Akt at Ser473 results, we observed a reduced level of p-GSK3β at Ser9 in the $A\beta_{1-42}$-injected mice compared with the control mice. Anthocyanin and anthocyanin-loaded PEG-AuNP (12 μg/g/day for 14 days) treatments significantly increased the level of p-GSK3β at Ser9 in the $A\beta_{1-42}$-injected mice compared with the mice injected with only $A\beta_{1-42}$ (Fig. 7). We also examined the tau hyperphosphorylation at Ser 404 and 413. Our immunoblot results showed that anthocyanins and anthocyanin-loaded PEG-AuNPs (12 μg/g/day for 14 days) treatment significantly reduced the level of p-tau at Ser 413 and Ser 404 in the $A\beta_{1-42}$-injected mice compared with mice injected with only $A\beta_{1-42}$ (Fig. 7).

## Anthocyanin-Loaded PEG-AuNPs Attenuated $A\beta_{1-42}$-Induced Neurodegeneration

The activation of the neuronal survival of the p-PI3-K/p-Akt pathway prevents Aβ-induced neurodegeneration by

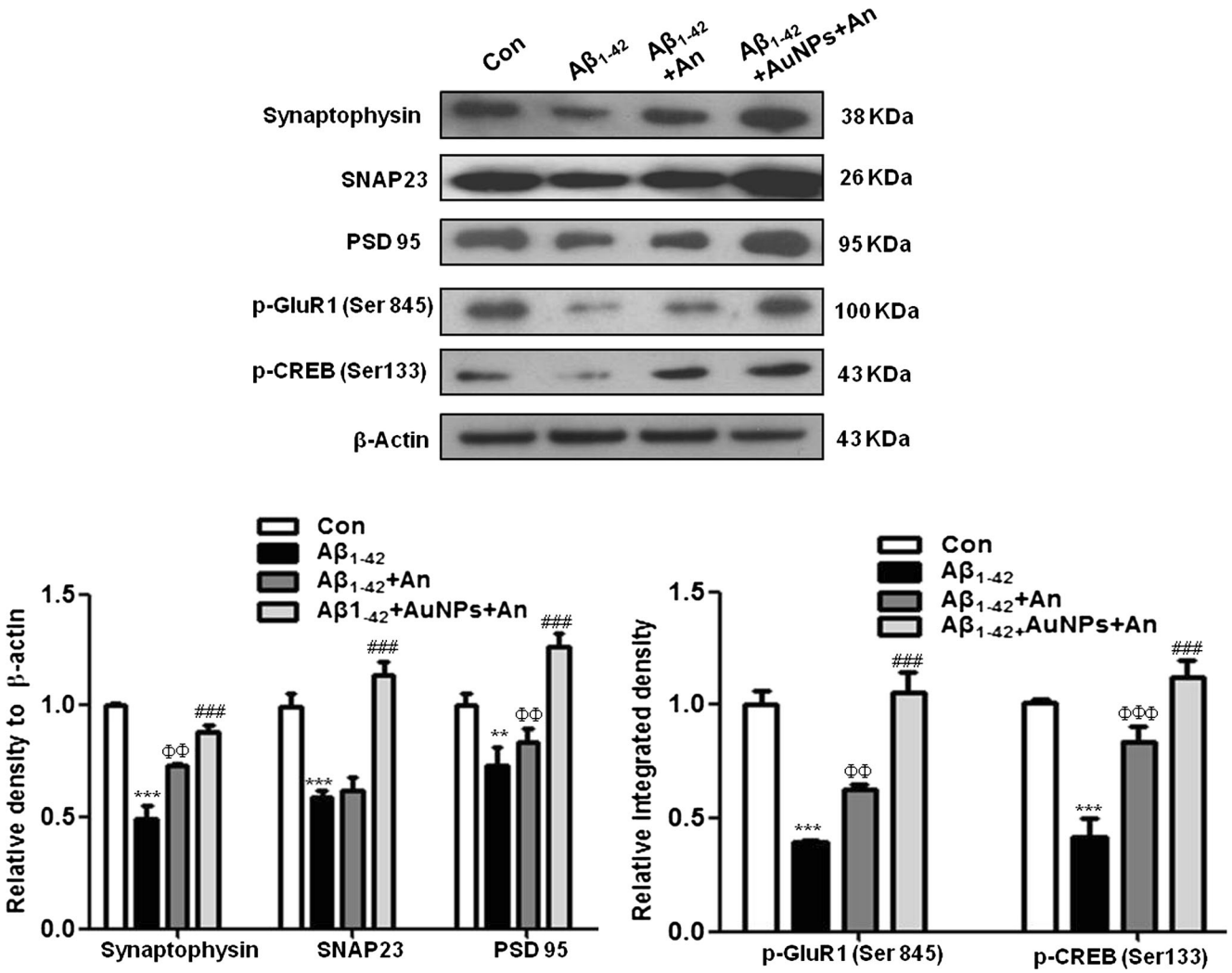


**Fig. 6** Anthocyanin-loaded PEG-AuNPs mitigated $A\beta_{1–42}$-induced synaptic dysfunction. The western blot bands of synaptophysin, SNAP23, PSD95, p-GluR1 (Ser 845), and p-CREB (Ser 133) in the hippocampus of the mice. The bands were quantified using the Sigma Gel software, and the differences are represented by a histogram. β-actin was used as a loading control. The density values are expressed in arbitrary units (A.U.) as the mean ± SEM for the, respectively, indicated protein ($n$ = 10 mice/group). The *asterisk* indicates the significant differences compared to the vehicle-treated control group, while the *phi sign* and *pound sign* indicate the significant differences compared to the $A\beta_{1–42}$-injected groups. Significance at $^{***}p < 0.001$, $^{\Phi\Phi}p < 0.01$, $^{\Phi\Phi\Phi}p < 0.001$, and $^{\#\#\#}p < 0.001$

activating anti-apoptotic proteins and preventing the expression of apoptotic markers [50]. It has been shown that $A\beta_{1–42}$ reduced Bcl2 and increased the Bax (Bax/Bcl2) ratio and Cyt c, which triggers caspases [29]. Our results indicated that $A\beta_{1–42}$ injection increased the ratio of Bax/Bcl2 and Cyt c, which was reversed by anthocyanins and anthocyanin-loaded PEG-AuNPs (12 μg/g/day for 14 days); however, the anthocyanin-loaded PEG-AuNPs (12 μg/g/day for 14 days) were more effective than anthocyanins alone (Fig. 8a). Caspases are key molecules of the apoptotic cascade, and caspase-9 is considered as an initiator caspase, while caspase-3 is an executive caspase [51]. We examined the apoptotic cascade of protein expression via western blot. The expression levels of caspase-9 and cleaved caspase-3 were elevated in the $A\beta_{1–42}$-injected mice compared with the control mice. Interestingly, both anthocyanins and anthocyanin-loaded PEG-AuNPs (12 μg/g/day for 14 days) reversed the elevated expression levels and significantly reduced the caspase-9 and cleaved caspase-3 levels in the $A\beta_{1–42}$-injected mice compared with mice injected with only $A\beta_{1–42}$ (Fig. 8a). The Aβ peptide has been shown to overactivate PARP-1, which leads to DNA damage and, as a result, neurodegeneration in the adult rat hippocampus [52]. We also detected an increase in cleaved PARP-1 in the hippocampus of $A\beta_{1–42}$-injected mice, which may be involved in the observed apoptosis and neurodegeneration. However, the anthocyanin and anthocyanin-loaded PEG-AuNP (12 μg/g/day for 14 days) treatments significantly reduced the levels of PARP-1 in the hippocampus

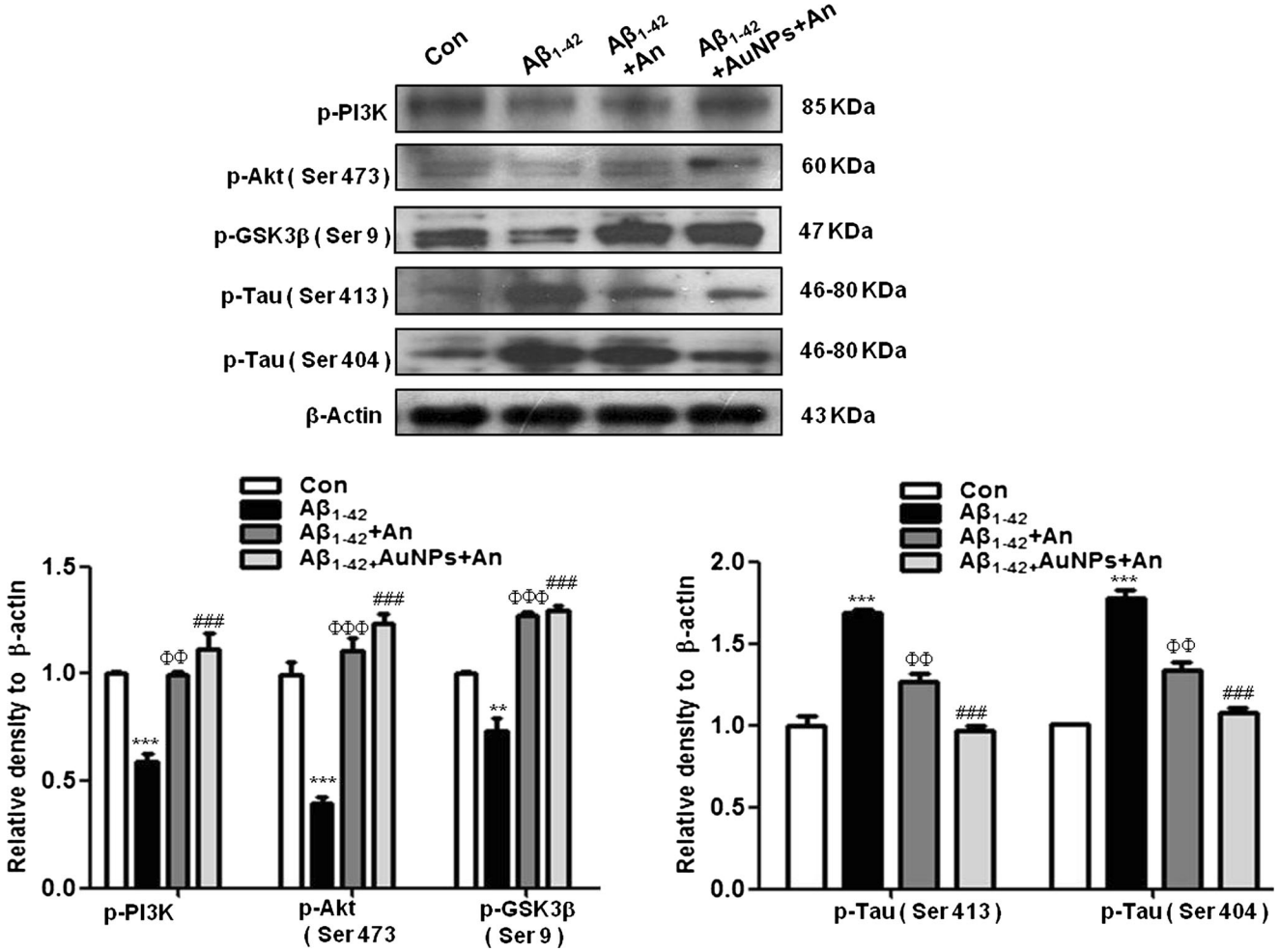


**Fig. 7** Anthocyanin-loaded PEG-AuNPs regulated $A\beta_{1-42}$-induced dysregulated PI3-K/Akt/p-GSK-3β signaling and prevented tau phosphorylation at Ser 413 and Ser 404. The western blot analysis of p-PI3K, p-Akt (Ser 473), p-GSK3β (Ser 9), p-tau Ser 413, and p-tau 404 in the hippocampus of mice. The bands were quantified using the Sigma Gel software, and the differences are represented by a histogram. β-actin was used as a loading control. The density values are expressed in arbitrary units (A.U.) as the mean ± SEM of the, respectively, indicated protein ($n$ = 10 mice/group). The *asterisk* indicates the significant differences compared to the vehicle-treated control group, while the *phi sign* and *pound sign* indicate the significant differences from the $A\beta_{1-42}$-injected groups. Significance at $^{**}p < 0.01$, $^{***}p < 0.001$, $^{\Phi\Phi}p < 0.01$, $^{\Phi\Phi\Phi}p < 0.001$, and $^{\#\#\#}p < 0.001$

of $A\beta_{1-42}$-injected mice compared with mice injected with only $A\beta_{1-42}$ (Fig. 8a). Immunohistochemical Nissl staining was performed to observe the neurodegeneration in experimental mice. The morphology shows that numbers of surviving neurons in the DG, CA3, and CA1 regions of the hippocampus were significantly decreased in the $A\beta_{1-42}$-injected mice compared with control mice. Treatment with anthocyanin-loaded PEG-AuNPs (12 μg/g/day for 14 days) ameliorated the effects of $A\beta_{1-42}$ and significantly increased the number of surviving neurons compared with mice injected with only $A\beta_{1-42}$ (Fig. 8b). Immunohistochemical FJB staining also revealed that the anthocyanin-loaded PEG-AuNPs (12 μg/g/day for 14 days) significantly reduced the $A\beta_{1-42}$-induced degenerated neuronal cells in the hippocampus and cortex (Fig. 8c).

## Discussion

The crossing of the BBB and controlled released are challenges for effective drug therapy that can be used for treatment of progressive neurodegenerative disorders. Nanotechnology and nanomedicine approaches to cross the BBB and allow for the controlled release of drugs are an emerging area of research in the field of neurotherapeutics. In this study, we prepared and characterized the conjugation of natural flavonoid anthocyanins with PEG-AuNPs to enhance the neuroprotective efficacy of the anthocyanins. We demonstrated that anthocyanin-loaded PEG-AuNPs enhanced the neuroprotective efficacy of anthocyanins against $A\beta_{1-42}$-induced memory deficits, synaptic impairments, and neuronal disorders.

The primary goal of this study was to prepare and characterize anthocyanin-loaded PEG-AuNPs. After evaluating the

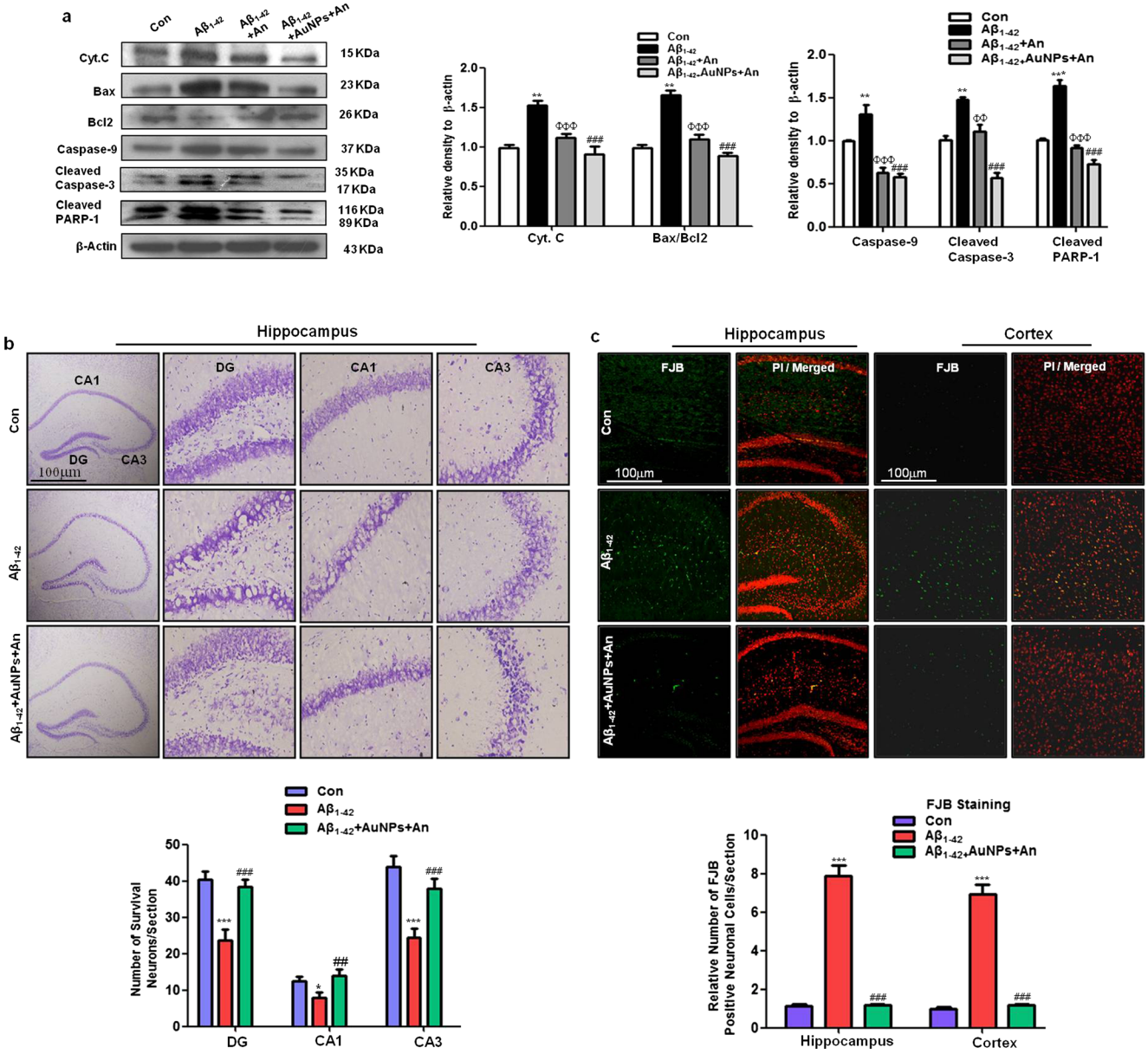


**Fig. 8** Anthocyanin-loaded PEG-AuNPs attenuated $A\beta_{1–42}$-induced neurodegeneration. **a** Western blot analysis of mouse hippocampus using Bcl2, Bax, cytochrome *c*, caspase-9, caspase-3, and cleaved PARP-1 antibodies. The bands were quantified using the Sigma Gel software, and the differences are represented by a histogram. Anti-β-actin was used as a loading control. The density values are expressed in arbitrary units (A.U.) as the mean ± SEM of the, respectively, indicated hippocampus proteins ($n$ = 10 mice/group). The *asterisk* indicates the significant differences from the vehicle-treated control group, while the *phi sign* and *pound sign* indicate the significant differences from the $A\beta_{1–42}$-injected groups. Significance at $^{**}p < 0.01$, $^{***}p < 0.001$, $^{\Phi\Phi}p < 0.01$, $^{\Phi\Phi\Phi}p < 0.001$, and $^{\#\#\#}p < 0.001$. **b** Representative images of immunohistochemical staining of Nissl in the DG, CA3, and CA1 regions of the hippocampus of the experimental mice. Magnifications are ×4 and ×20; *scale bar* = 100 μm. **c** Representative images of immunohistochemical staining of FJB in the hippocampus and cortex of the mice. Magnification ×10, *scale bar* = 100 μm. The data are expressed as the means ± SEM. The *asterisk* indicates the significant differences compared to the vehicle-treated control group, while the *pound sign* indicates the significant differences from the $A\beta_{1–42}$-injected groups. Significance at $^{*}p < 0.05$, $^{***}p < 0.001$, and $^{\#\#\#}p < 0.001$

safety profile of the PEG-AuNPs, we conjugated anthocyanins with PEG-AuNPs, which was determined and confirmed through FTIR analyses. The physical stability of the particles was assessed by analyzing the particle size, its distribution, and the charge produced on the anthocyanin-loaded PEG-AuNPs through TEM, DLS, and a zetasizer system. The results showed that the particles exhibited a uniformly sized, non-aggregated spherical shape and were well dispersed with a mean particle size of approximately 135 ± 5 nm and a zeta potential of −11.5 ± 2 mV (Fig. 2b–d), which indicated that the conjugation of the anthocyanins with PEG-AuNPs was of good reproducible quality preparations. Therefore, we further

used these anthocyanin-loaded PEG-AuNPs and free anthocyanins against $A\beta_{1-42}$-induced neurotoxicity.

Here, we observed impairments in spatial working memory, as evidenced by a longer escape latency during the training session, decreased time spent in the target quadrant, a decreased number of platform crossings during the probe test, and a significant reduction in the spontaneous alteration behavior percent in the $A\beta_{1-42}$-injected mice. We investigated the neuroprotective effect of anthocyanin-loaded PEG-AuNPs and free anthocyanins (12 μg/g/day for 14 days), which are natural polyphenolic compounds found in various plants and edible fruits. We observed that treatments with free anthocyanins and anthocyanin-loaded PEG-AuNPs (12 μg/g/day for 14 days) ameliorated $A\beta_{1-42}$-triggered memory deficits (Fig. 4a–d).

Synaptic impairment and loss have been implicated in AD patients and animal models of AD [53]. Aβ-induced synaptotoxicity has been associated with decreased levels of synaptophysin and PSD95 [54, 55]. We also examined that i.c.v. $A\beta_{1-42}$-injected mice showed significantly reduced levels of the pre-synaptic protein synaptophysin and post-synaptic protein PSD95 in the hippocampus. The levels of SNAP-23 and p-AMPAR (Ser 845) were decreased in our $A\beta_{1-42}$-injected mice, which is consistent with previous studies in which these post-synaptic markers were decreased in the AD model [56]. Importantly, studies show that PSD95 and SNAP-23 play valuable roles in the regulation of AMPAR trafficking [57, 58]. Another memory-related transcription factor, p-CREB (Ser 133), is implicated in memory and synaptic functions, and the inhibition or reduction of p-CREB (Ser 133) levels impaired hippocampus-associated memory function [59, 60]. We also investigated the reduced p-CREB (Ser 133) level in the $A\beta_{1-42}$-injected group. The decreased expression of synaptic markers may be associated with memory impairment in the $A\beta_{1-42}$-injected mice. Our results are consistent with a previous study of synaptic disorder and synaptic loss in $A\beta_{1-42}$-induced neurodegeneration [56]. Anthocyanin and anthocyanin-loaded PEG-AuNP treatments ameliorated the effect of $A\beta_{1-42}$ and prevented synaptic dysfunction by increasing the levels of pre-synaptic (synaptophysin) and post-synaptic (PSD95, SNAP-23, p-AMPARs (Ser 845), and p-CREB (Ser133)) protein in the $A\beta_{1-42}$-injected mice (Fig. 6).

Aβ exposure directly affects the PI3K/Akt/GSK3β neuroprotective and survival pathway, which is also impaired in the amyloid precursor protein/presenilin-1 (APP/PS1) double transgenic AD mouse model of AD [61]. It has been reported that activated p-PI3K/p-Akt pathways regulated numerous downstream proteins and are involved in the neuroprotection and neuronal survival pathways of Bcl-2 family members, such as caspase-9, caspase-3, and, importantly, the GSK3β protein kinase [62, 63], which also plays a role in tau hyperphosphorylation [64]. Based on previously published studies, we hypothesized that the PI3K/Akt/GSK3β signaling pathway may be involved in the anthocyanin-mediated neuroprotection against $A\beta_{1-42}$-induced neurotoxicity. Our results showed that Akt phosphorylation at Ser 473 was significantly reduced, activating GSK3β in the $A\beta_{1-42}$-injected mice; however, anthocyanins and anthocyanin-loaded PEG-AuNPs activated the p-PI3K/p-Akt pathway and prevented the activation of GSK3β by increasing the phosphorylation of p-GSK3β at Ser 9. GSK-3β is a ubiquitous and abundant kinase in the brain, mediating the phosphorylation of numerous proteins such as tau [65]. GSK-3β-overexpressing transgenic mice exhibit tau hyperphosphorylation, neurodegeneration, and memory impairment [66, 67]. Additionally, lithium chloride, a GSK-3β inhibitor, attenuated Aβ accumulation and plaque formation [68]. Aβ exposure affects neurons, leading to apoptosis, neuronal degeneration, and hyperphosphorylation of tau protein [69]. Elegant studies have shown that $A\beta_{1-42}$-induced tau hyperphosphorylation may be due to the modulation of several kinases, including cyclidine-dependent kinase-5, GSK-3β, p388/MAPK, JANK, and ERK. Of these kinases, GSK3β is the key mediator kinase that is associated with tau phosphorylation at Ser 413/404 [70]. Consistent with previous studies, our results also showed that the p-GSK3β (Ser 9) level was decreased in the $A\beta_{1-42}$-injected mice, which activated GSK3β and also likely increased tau hyperphosphorylation at Ser 413 and 404. Anthocyanins and anthocyanin-loaded PEG-AuNPs activate the phosphorylation of GSK3β at Ser 9, thereby possibly preventing GSK-3β-dependent tau hyperphosphorylation at Ser 413 and 404.

Previous studies have reported Aβ-mediated apoptosis and neurodegeneration [71, 72]. Caspases, which are activated by Aβ exposure, have been implicated in apoptosis and neurodegeneration [73]. Activated caspases overexpressed PARP-1, which triggered apoptosis and neurodegeneration [74]. Love et al. reported increased PARP-1 levels in AD, which was implicated in decreasing the oxidized nicotinamide adenine dinucleotide ($NAD^+$) levels and led to apoptosis and neurodegeneration [75]. These results showed that anthocyanins and anthocyanin-loaded PEG-AuNPs attenuated the overexpression of activated caspases and halt PARP-1 cleavage, indicating that anthocyanins and anthocyanin-loaded PEG-AuNPs prevented $A\beta_{1-42}$-induced apoptotic neuronal cell death in the $A\beta_{1-42}$-injected mice. Additionally, the results of the immunohistochemical Nissl and FJB staining analysis were consistent with the immunoblot results, showing that anthocyanin-loaded PEG-AuNPs attenuated $A\beta_{1-42}$-induced neurodegeneration (Fig. 8b, c).

To the best of our knowledge, this work is the first in vivo study of anthocyanin-loaded PEG-AuNPs in an $A\beta_{1-42}$ mouse model of AD. Importantly, the anthocyanin-loaded PEG-AuNPs were more effective than free anthocyanins against $A\beta_{1-42}$-induced neurotoxicity, suggesting that the

PEG-AuNPs enhanced the bioavailability and controlled the release of the anthocyanins in the $A\beta_{1-42}$-injected mice. Moreover, our results demonstrated the neuroprotective effect of anthocyanins and anthocyanin-loaded PEG-AuNPs against $A\beta_{1-42}$-triggered memory deficits, synaptic dysfunction, and neurodegeneration. Taken together, our results indicate that the polyphenolic flavonoid anthocyanins are important neuroprotective dietary supplements that are beneficial to human health by ameliorating age-associated neurodegenerative diseases such as AD. Importantly, anthocyanin's conjugation with PEG-AuNPs is an emerging and interesting research topic that provides new avenues in the fields of nanomedicine for studying progressive age-related neurodegenerative diseases such as AD.

**Acknowledgments** This research was supported by the Pioneer Research Center and Brain Research Program through the National Research Foundation of Korea funded by the Ministry of Science, ICT and Future Planning (2012-0009521 and 2016M3C7A1904391).

**Compliance with Ethical Standards** All methods complied with the guidelines (approval ID 125) of the animal ethics committee (IACUC) of the Division of Applied Life Sciences, Department of Biology at Gyeongsang National University, South Korea.

**Conflict of Interest** The authors declare that they have no conflict of interest.

## References

1. Mattson MP (2004) Pathways towards and away from Alzheimer's disease. Nature 430:631–639
2. Abramov E, Dolev I, Fogel H, Ciccotosto GD, Ruff E, Slutsky I (2009) Amyloid-beta as a positive endogenous regulator of release probability at hippocampal synapses. Nat Neurosci 12:1567–1576
3. Butterfield DA, Drake J, Pocernich C, Castegna A (2001) Evidence of oxidative damage in Alzheimer's disease brain: central role for amyloid beta-peptide. Trends Mol Med 7:548–554
4. Suen KC, Lin KF, Elyaman W, So KF, Chang RC, Hugon J (2003) Reduction of calcium release from the endoplasmic reticulum could only provide partial neuroprotection against beta-amyloid peptide toxicity. J Neurochem 87:1413–1426
5. Russell CL, Semerdjieva S, Empson RM, Austen BM, Beesley PW, Alifragis P (2012) Amyloid-β acts as a regulator of neurotransmitter release disrupting the interaction between synaptophysin and VAMP2. PLoS One 7:e43201. doi:10.1371/journal.pone.0043201
6. Kim HG, Kim JY, Whang WW, Oh MS (2014) Neuroprotective effect of Chunghyuldan from amyloid beta oligomer induced neuroinflammation in vitro and in-vivo. Can J Physiol Pharmacol 92:429–437
7. Begley DJ (2004) Delivery of therapeutic agents to the central nervous system: the problems and the possibilities. Pharmacol Ther 104:29–45
8. Wohlfart S, Gelperina S, Kreuter J (2012) Transport of drugs across the blood-brain barrier by nanoparticles. J Control Release 161:264–273
9. Gibson JD, Khanal BP, Zubarev ER (2007) Paclitaxel-functionalized gold nanoparticles. J Am Chem Soc 129:11653–11661
10. Khan MS, Vishakante GD, Siddaramaiah H (2013) Gold nanoparticles: a paradigm shift in biomedical applications. Adv Colloid Interf Sci 199-200:44–58
11. Jain PK, Huang X, El-Sayed IH, El-Sayed MA (2008) Noble metals on the nanoscale: optical and photothermal properties and some applications in imaging, sensing, biology, and medicine. Acc Chem Res 41:1578–1586
12. Ghosh P, Han G, De M, Kim CK, Rotello VM (2008) Gold nanoparticles in delivery applications. Adv Drug Deliv Rev 60:1307–1315
13. Lasagna-Reeves C, Gonzalez-Romero D, Barria MA, Olmedo I, Clos A, Sadagopa Ramanujam VM et al (2010) Bioaccumulation and toxicity of gold nanoparticles after repeated administration in mice. Biochem Biophys Res Commun 393:649–655
14. Hillyer JF, Albrecht RM (2001) Gastrointestinal persorption and tissue distribution of differently sized colloidal gold nanoparticles. J Pharm Sci 90:1927–1936
15. Sonavane G, Tomoda K, Makino K (2008) Biodistribution of colloidal gold nanoparticles after intravenous administration: effect of particle size. Colloids Surf B Biointerfaces 66:274–280
16. Jong WHD, Hagens WI, Krystek P, Burger MC, Sips AJAM, Geertsma RE (2008) Particle size-dependent organ distribution of gold nanoparticles after intravenous administration. Biomaterials 29:1912–1919
17. Malka S, Menachem M, Panet H, Rachela P (2014) Transport of nanoparticles through the blood–brain barrier for imaging and therapeutic applications. Nanoscale. doi:10.1039/c3nr04878k
18. Sousa F, Mandal S, Garrovo C, Astolfo A, Bonifacio A, Latawiec D et al (2010) Functionalized gold nanoparticles: a detailed in vivo multimodal microscopic brain distribution study. Nanoscale 2:2826–2834
19. Roney C, Kulkarni P, Arora V, Antich P, Bonte F, Wu A et al (2005) Targeted nanoparticles for drug delivery through the blood–brain barrier for Alzheimer's disease. J Control Release 108:193–214
20. Soppimath KS, Aminabhavi TM, Kulkarni AR, Rudzinski WE (2001) Biodegradable polymeric nanoparticles as drug delivery devices. J Control Release 70:1–20
21. Niidome T, Yamagata M, Okamoto Y, Akiyama Y, Takahashi H, Kawano T et al (2006) PEG-modified gold nanorods with a stealth character for in vivo applications. J Control Release 114:343–347
22. Harris JM, Chess RB (2003) Effect of PEGylation on pharmaceuticals. Nat Rev Drug Discov 2:214–221
23. Shukitt-Hale B, Cheng V, Joseph JA (2009) Effects of blackberries on motor and cognitive function in aged rats. Nutr Neurosci 12:135–140
24. Rio DD, Borges G, Crozier A (2010) Berry flavonoids and phenolics: bioavailability and evidence of protective effects. Br J Nutr 104:S67–S90
25. Ullah I, Park HY, Kim MO (2014) Anthocyanins protect against kainic acid-induced excitotoxicity and apoptosis via ROS-activated AMPK pathway in hippocampal neurons. CNS Neurosci Ther 20:327–338
26. Shah SA, Yoon GH, Kim MO (2015) Protection of the developing brain with anthocyanins against ethanol-induced oxidative stress and neurodegeneration. Mol Neurobiol 51:1278–1291
27. Rehman SU, Shah SA, Ali T, Chung JI, Kim MO (2016) Anthocyanins reversed D-galactose-induced oxidative stress and neuroinflammation mediated cognitive impairment in adult rats. Mol Neurobiol. doi:10.1007/s12035-015-9604-5
28. Khan MS, Ali T, Kim MW, Jo MH, Jo MG, Badshah H et al (2016) Anthocyanins protect against LPS-induced oxidative stress-mediated neuroinflammation and neurodegeneration in the adult mouse cortex. Neurochem Int 100:1–10. doi:10.1016/j.neuint.2016.08.005
29. Badshah H, Kim TH, Kim MO (2015) Protective effects of anthocyanins against amyloid beta-induced neurotoxicity in vivo and in vitro. Neurochem Inti 80:51–59

30. Sawant VJ, Bamane SR (2013) PEG encapsulated curcumin conjugated cobalt ferrite core shell nanoassembly for biocompatibility testing and drug delivery. Int J Pharm Sci Rev Res 27:159–164
31. Akhtar F, Rizvi MMA, Rizvi MM, Kar SK (2012) Oral delivery of curcumin bound to chitosan nanoparticles cured *Plasmodium yoelii* infected mice. Biotechnol Adv 30:310–320
32. Manju S, Sreenivasan K (2012) Gold nanoparticles generated and stabilized by water soluble curcumin-polymer conjugate: blood compatibility evaluation and targeted drug delivery onto cancer cells. J Colloid Interface Sci 368:144–151
33. Gangwar RK, Dhumale VA, Kumari DB, Nakate UT, Gosavi SW, Sharma RB et al (2012) Conjugation of curcumin with PVP capped gold nanoparticles for improving bioavailability. Mat Sci and Eng C 32:2659–2663
34. Bretteville A, Marcouiller F, Julien C, Khoury NBE, Petry FR, Poitras I et al (2012) Hypothermia-induced hyperphosphorylation: a new model to study tau kinase inhibitors. Sci Rep 2:480. doi:10.1038/srep00480
35. Shah M, Ullah N, Choi MH, Kim MO, Yoon SC (2012) Amorphous amphiphilic P(3HV-co-4HB)-b-mPEG block copolymer synthesized from bacterial copolyester via melt transesterification: nanoparticle preparation, cisplatin-loading for cancer therapy and in vitro evaluation. Eur J Pharm Biopharm 80(3):518–527
36. Ali T, Badshah H, Kim T, Kim MO (2015) Melatonin attenuates D-galactose-induced memory impairment, neuroinflammation and neurodegeneration via RAGE/NF-$_K$B/JNK signaling pathway in aging mouse model. J Pineal Res 58:l71–l85
37. Ahmad A, Ali T, Park HY, Badshah H, Rehman SU, Kim MO (2016) Neuroprotective effect of fisetin against amyloid beta-induced cognitive/synaptic dysfunction, neuroinflammation and neurodegeneration in adult mice. Mol Neurobiol. doi:10.1007/s12035-016-9795-4
38. Badshah H, Ali T, Rehman SU, Amin FU, Ullah F, Kim TH et al (2015) Protective effect of lupeol against lipopolysaccharide-induced neuroinflammation via the p38/c-jun N-terminal kinase pathway in the adult mouse brain. J Neuroimmune Pharamacol 11:48–60
39. Shah SA, Yoon GH, Chung SS, Abid MN, Kim TH, Lee HY et al (2016) Novel osmotin inhibits SREBP2 via the AdipoR1/AMPK/SIRT1 pathway to improve Alzheimer's disease neuropathological deficits. Mol Psychiatry. doi:10.1038/mp.2016.23
40. Badshah H, Ali T, Kim MO (2016) Osmotin attenuates LPS-induced neuroinflammation and memory impairments via the TLR4/NF$_K$ signalling pathway. Sci Rep 6:24493. doi:10.1038/srep24493
41. Badshah H, Kim TH, Kim MJ, Ahmad A, Ali T, Yoon GH et al (2014) Apomorphine attenuates ethanol-induced neurodegeneration in the adult cortex. Neurochem Int 74:8–15
42. Ullah F, Ali T, Ullah N, Kim MO (2015) Caffeine prevents D-galactose-induced cognitive deficits, oxidative stress, neuroinflammation and neurodegeneration in the adult rat brain. Neurochem Int 90:114–124
43. Bouzas V, Haller T, Hobi N, Felder E, Pastorize-Santos I, Perez-Gil J (2013) Nontoxic impact of PEG-coated gold nanospheres on functional pulmonary surfactant-secreting alveolar type II cells. Nanotoxicology 8:813–823
44. Guglielmotto M, Monteleone D, Giliberto L, Fornaro M, Borghi R, Tamagno E et al (2011) Amyloid-$\beta_{42}$ activates the expression of BACE1 through the JNK pathway. J Alzheimers Dis 27:871–883
45. Ali T, Kim MO (2015) Melatonin ameliorates amyloid beta-induced memory deficits, tau hyperphosphorylation and neurodegeneration via PI3/Akt/Gsk3β pathway in the mouse hippocampus. J Pineal Res. doi:10.1111/jpi.12238
46. Ali T, Yoon GH, Shah SA, Lee HY, Kim MO (2015) Osmotin attenuates amyloid beta-induced memory impairment, tau phosphorylation and neurodegeneration in the mouse hippocampus. Sci Rep. doi:10.1038/srep11708
47. Minano-Molina AJ, Espana J, Martin E, Barneda-Zahonero B, Fado R, Sole M (2011) Soluble oligomers of amyloid-β peptide disrupt membrane trafficking of α-amino-3-hydroxy-5-methylisoxazol-4-propionic acid receptor contributing to early synapse dysfunction. J Biol Chem 286:27311–27321
48. Tokutake T, Kasuga K, Yajima R, Sekine Y, Tezuka T, Nishizawa M et al (2012) Hyperphosphorylation of tau induced by naturally secreted amyloid-β at nanomolar concentrations is modulated by insulin-dependent Akt-GSK3β signaling. J Biol Chem 287:35222–35233
49. Salkovic-Petrisic M, Tribl F, Schmidt M, Hoyer S, Riederer P (2006) Alzheimer-like changes in protein kinase B and glycogen synthase kinase-3 in rat frontal cortex and hippocampus after damage to the insulin signaling pathway. J Neuroch 96:1005–1015
50. Bhaskar K, Miller M, Chludzinski A, Herrup K, Zagorski M, Lamb BT (2009) The PI3K-Akt-mTOR pathway regulates Aβ oligomer induced neuronal cell cycle events. Mol Neurodegener. doi:10.1186/1750-1326-4-14
51. Li J, Wang G, Liu J, Zhou L, Dong M, Wang R et al (2010) Puerarin attenuates amyloid-beta-induced cognitive impairment through suppression of apoptosis in rat hippocampus in vivo. Eur J Pharmacol 649:195–201
52. Strosznajder JB, Jesko H, Stroznnajder RP (2000) Effect of amyloid beta peptide on poly (ADP-ribose) polymerase activity in adult and aged rat hippocampus. Acta Biochim Pol 47:847–854
53. Hemar A, Mulle C (2011) Alzheimer's disease, amyloid peptide and synaptic dysfunction. Medicine. Science 27:733–736
54. Ahmad T, Enam SA, Gillani AH (2010) Curcumonoids enhances memory in an amyloid-infused rat model of Alzheimer's disease. Neuroscience 169:296–1306
55. Canas PM, Porciuncula LO, Cunha GMA, Silva CG, Machado NJ, Oliveira JMA et al (2009) Adenosine $A_{2A}$ receptor blockade prevents synaptotoxicity and memory dysfunction caused by β-amyloid peptides via p38 mitogen-activated protein kinase pathway. J Neurosci 29:14741–14751
56. Tu S, Okamoto S, Lipton SA, Xu H (2014) Oligomeric Aβ-induced synaptic dysfunction in Alzheimer's disease. Mol Neurodegener 9:48. doi:10.1186/1750-1326-9-48
57. Ehrlich I, Malinow R (2004) Postsynaptic density 95 controls AMPA receptor incorporation during long-term potentiation and experience-driven synaptic plasticity. J Neurosci 24(4):916–927
58. Suh YH, Terashima A, Petralima RS, Wenthold RJ, Isaac JTR, Roche KW, Roche PA (2010) A neuronal role for SNAP23 in postsynaptic glutamate receptor trafficking. Nat Neurosci 13:338–343
59. Barco A, Marie H (2011) Genetic approaches to investigate the role of CREB in neuronal plasticity and memory. Mol Neurobiol 44:330–349
60. Restivo L, Tafi E, Ammassari-Teule M, Marie H (2009) Viral mediated expression of a constitutively active form of CREB in hippocampal heurons increases memory. Hippocampus 19:228–234
61. Jimenez S, Torres M, Vizuete M, Sanchez-Varo R, Sanchez-Mejias E, Trujillo-Estrada L et al (2011) Age-dependent accumulation of soluble beta (Abeta) oligomers reverses neuroprotectvive effect of soluble amyloid precursor protein-alpha (sAPP(alpha)) by modulating phosphatidylinositol 3-kinase (PI3K)/Akt-GSK-3beta pathway in Alzheimer mouse model. J B Chem 286:18414–18425
62. Datta SR, Brunet A, Greenberg ME (1999) Cellular survival: a play in three Akt. Genes Dev 13:2905–2927
63. Song G, Ouyang G, Bao S (2005) The activation of Akt/PKB signaling pathway and cell servival. J Cell Mol Med 9:59–71
64. Hooper C, Killick R, Lovestone S (2008) The GSK3 hypothesis of Alzheimer's disease. J Neurochem 104:1433–1439
65. Avila J, Leon-Espinosa G, Garcia E, Garcia-Escudero V, Hernandez F, Defelipe J (2012) Tau phosphorylation by GSK3 in different

conditions. Int J Alzheimers Dis 2012:578373. doi:10.1155/2012/578373

66. Engel T, Hernandez F, Avila J, Lucas JJ (2006) Full reversal of Alzheimer's disease-like phenotype in a mouse model with conditional overexpression of glycogen synthase kinase-3. J Neurosci 25: 5083–5090
67. Lucas JJ, Hernandez F, Gomez-Ramos P, Moran MA, Hen R, Avila J (2001) Decreased nuclear beta-catenin, tau hyperphosphorylation and neurodegeneration in GSK-3beta conditional transgenic mice. EMBO J 20:27–39
68. Sofola O, Kerr F, Rogers I, Killick R, Augustin H, Gandy C et al (2010) Inhibition of GSK-3 ameliorates Abeta pathology in an adult-onset *Drosophila* model of Alzheimer's disease. PLoS Genet 6:e1001087
69. Kar S, Slowikowski SP, Westaway D, Mount HTJ (2004) Interactions between beta-amyloid and central cholinergic neurons: implications for Alzheimer's disease. J Psychiatry Neurosci 29:427–441
70. Mazanetz MP, Fischer PM (2007) Untangling tau hyperphosphorylation in drug design for neurodegenerative disease. Nature Reviews 6:464–479
71. Cancino LG, Toledo EM, Leal NR, Hernandez DE, Yavenes LF, Inestrosa NC et al (2008) STI571 prevents apoptosis, tau phosphorylation and behavioral impairments induced by Alzheimer's β-amyloid deposits. Brain 131:2425–2442
72. Lauren J, Gimbel DA, Nygaard HB, Gilbert JW, Strittmatter SM (2009) Cellular prion protein mediates impairment of synaptic plasticity by amyloid-β oligomers. Nature 457:1128–1132
73. Zussy C, Brureau A, Delair B, Marchal S, Keller E, Ixart G et al (2011) Time-course and regional analysis of the physiopathological changes induced after cerebral injection of amyloid β fragment in rats. Am J Pathol 179:315–334. doi:10.1016/j.ajpath
74. Sairanen T, Szepesi R, Karjalainen-lindsberg ML, Saksi J, Paettu A, Lindsberg PJ (2009) Neuronal caspase-3 and PARP-1 correlate differentially with apoptosis and necrosis in ischemic human stroke. Acta Neuropatho 118:541–552
75. Love S, Barber R, Wilcock GK (1999) Increased poly (ADP-ribosyl) ation of nuclear proteins in Alzheimer's disease. Brain 122:247–256